Preparation and Characterization of Polyaniline (PANI) doped-$Li_3V_2(PO_4)_3$

Guoqing Zhang[1], Xinxi Li[1], Haitao Jia[2], Xiuxiu Pang[2], Hongwei Yang[2], Yahui Wang[2], Keqiang Ding[2]*

[1]Faculty of Materials and Energy, Guangdong University of Technology, Guangzhou 510006, R. P. China
[2] College of Chemistry and Materials Science, Hebei Normal University, Shijiazhuang, Hebei 050016, P.R. China
[*]E-mail: dkeqiang@263.net

For the first time, aniline was doped into the precursors used for preparing $Li_3V_2(PO_4)_3$, leading to a polyanilne (PANI)-doped $Li_3V_2(PO_4)_3$. In this work, three samples, having the weight content of aniline 5 wt%, 7 wt% and 10wt%, respectively, were fabricated. The as-prepared samples were characterized by XRD, SEM, and FTIR, respectively. Unfortunately, the obtained XRD patterns of pure $Li_3V_2(PO_4)_3$ is not very similar to the standard XRD patterns of $Li_3V_2(PO_4)_3$. But the XRD patterns of the PANI-doped $Li_3V_2(PO_4)_3$ are consistent with standard XRD patterns of $Li_3V_2(PO_4)_3$ in some degree. SEM images strongly demonstrated that the weight content of aniline affected the morphologies of the obtained samples greatly, and it seemed that the sample with 7 wt % aniline has the smallest particle size among the obtained samples. Interestingly, the charge-discharge curves revealed that the PANI-doped sample of 7wt% aniline exhibited the largest discarge capacity among the three samples. The possible reasons for above phenomenon were well discussed based on the FTIR spectra and EIS measurement. Showing the sample of PANI-doepd $Li_3V_2(PO_4)_3$ is the main contribution of this work, though unsatisfactory results were acquired.

1. INTRODUCTION

Although Lithium cobalt oxide has been the positive electrode for commercial lithium secondary batteries, its high cost and toxicity prohibit its use in large-scale applications, especially in the field of electrical vehicles (EV) and hybrid electrical vehicles (HEV)[1]. Recently, a class of cathode materials, transition-metal phosphates, $LiMPO_4$ (M=Ni, Co, Mn) [2], $Li_3V_2(PO_4)_3$[3], and

$LiVPO_4F$[4], have been well developed as cathode materials for lithium batteries because of their remarkable electrochemical performance and thermal stability.

Phosphates monoclinic $Li_3V_2(PO_4)_3$ with both mobile Li cations and redox-active metalsites located with in a rigid phosphate frame work has intrigued considerable interest due to its stable frame work, higher operating voltage, and large theoretical capacity. It is reported that monoclinic lithium vanadium phosphate contains three independent lithium sites with a theoretical discharge capacity of 197mAh/g. However, as addressed in the very recently published papers, the lower electronic conductivity of $Li_3V_2(PO_4)_3$ leads to the poor electrode conductivity and cycling performance. Therefore, improving the electrochemical performance of $Li_3V_2(PO_4)_3$ is still a main task in the research field of cathode materials.

Generally, alien metal doping and carbon coating were regarded as the main methods for improving the electrochemical performance of $Li_3V_2(PO_4)_3$. For example, Tu et al [5]. has investigasted the Ag-doped $Li_3V_2(PO_4)_3$, and pointed out that the carbon and silver co-modification decreases the charge transfer resistance of $Li_3V_2(PO_4)_3/(Ag+C)$ cathode, and improves the conductivity and boosts the electrochemical performance of the electrode. Zhao's group [6] systematically probed the Co-doped $Li_3V_2(PO_4)_3$ prepared via a solid-state reaction, and indicated that the doping of Co^{2+} into V sites should be favorable for the structural stability of $Li_3V_{2-x}Co_x(PO_4)_3/C$ compounds and so moderate the volume changes (expansion/contraction) seen during the reversible Li^+ extraction/insertion, thus resulting in the improvement of cell cycling ability. Also, Chen [7] reported the synthesis and characterization of carbon-coated monoclinic $Li_3V_2(PO_4)_3$ (LVP) cathode materials, and inferred that the carbon coating can enhance the conductivity of the composite materials and hinder the growth of $Li_3V_2(PO_4)_3$ particles. While, to the best of our knowledge, there is no paper reporting the polyaniline-doped $Li_3V_2(PO_4)_3$.

Polyaniline (PANI) is an important conducting polymer due to its facile synthesis, environmental stability, and controllable physical and electrochemical properties by oxidation and protonation [8]. PANI has been used in cathode materials of the lithium secondary batteries [9, 10]. For example, Huang [11] has doped PANI into $LiFePO_4$, in which PANI was formed in situ by chemical oxidative polymerization using ammonium persulfate as an oxidizer, and revealed that the incorporated PANI can work not only as an additional host for Li^+-ion insertion/extraction, but also as a binder to modify the electrode surface and a container for electrolyte to penetrate into carbon coated $LiFePO_4$ particles.

In the present work, for the first time, based on our previous works on PANI[12], aniline was directly mixed with the precursors used for preparing $Li_3V_2(PO_4)_3$, after calcination at a desired temperature, the so-called PANI-doped $Li_3V_2(PO_4)_3$ was fabricated. Herein, three kinds of sample, i.e., 5 wt%, 7wt% and 10wt% PANI-doped samples, were prepared in the absence of inert gas flow. It should be noticed that a carbon-coated crucible was used in preparing the samles. The role of the weight percent of aniline in the precursor on the preparation of $Li_3V_2(PO_4)_3$, and on the electrochemical performance as well , were discussed.

2. EXPERIMENTAL

2.1. Materials

LiOH•H$_2$O, NH$_4$H$_2$PO$_4$, V$_2$O$_5$, aniline and oxalic acid were all purchased from Tianjin Chemical Reagent Co. Ltd. All materials used in the electrochemical measurement, such as acetylene black, polytetrafluoroethylene (PTFE) binder, electrolyte of 1 M LiClO$_4$ and the cell were all supported by the Tianjin Lianghuo S&T Developing Co. Ltd. All the chemicals were used as-received without any further treatment.

2.2. Preparation of PANI-doped Li$_3$V$_2$(PO$_4$)$_3$

Scheme 1. Photos for the samples obtained in preparing stages. Photo **a**: after being dried at 80º; photo **b**: sample dried at 300 º; photo **c**: the product of 7 wt% PANI-doped Li$_3$V$_2$(PO$_4$)$_3$.

Briefly, a proper amount of V_2O_5 was dissolved into a 0.5 M HCl solution, and then $LiOH \cdot H_2O$, $NH_4H_2PO_4$ and oxalic acid were mixed into the above solution, lastly, aniline was added into above solution. It should be noticed that the molar ratio of n(Li): n(V): n(P) : n(oxalic acid) is 3:2:3:2. The weight percent of aniline added was calculated based on the whole weight of the starting materials. The obtained blue solution was dried in an oven at around 80°C until loose and porous green powder was obtained (as shown by photo **a** in Scheme 1). The well ground powder was sintered in a muffle furnace at 300°C in air for about 4 hour, giving rise to black powders (as shown by photo **b** in Scheme 1). And then powder was ground again before being transferred into a crucible, which was covered by carbon powders (~10 g). Lastly, the well ground powder was sintered again at 800°C for around 4 hour, leading to powdery particles (as shown by photo **c** in Scheme 1). The aniline-free sample was also prepared using above method in the absence of aniline. Thus, four kinds of samples, i.e., aniline-free, 5 wt%, 7 wt% and 10wt%, respectively, were fabricated.

2.3. Characterization

X-ray diffraction (Bruker AXS, D8 ADVANCE, Germany) was used to examine the phase homogeneity. The particle morphology was observed by scanning electron microscopy (HITACHI, SEM S-570) and transmission electron microscopy (HITACHI, TEM H-7650). Energy dispersive spectrometer (EDS, INCA Energy 350, England) was employed to analyze the components of the as-prepared samples. Fourier transform infrared spectrometry (FT-IR) measurements are carried out on a Hitachi FT-IR-8900 spectrometer (Japan)

The cathodes used for the electrochemical characterization were fabricated by blending the prepared active material powders with acetylene black and polytetrafluoroethylene (PTFE) binder in a weight ratio of 85:10:5. Two-electrode electrochemical cells consisting of lithium metal foil as the negative electrode, Celgard 2400 separator, and an electrolyte of 1 M $LiClO_4$ in ethylene carbonate (EC):diethyl carbonate (DEC):dimethyl carbonate (DMC) (2:5:11, vol.) were assembled in a nitrogen-filled glove box. The electrochemical cycle tests were performed using a LAND series battery testing system (Wuhan Kinguo Electronics Co., Ltd. China) at various rates (1 C=197 mAh/g) between 3.0 and 4.8 V at room temperature.

3. RESULTS AND DISCUSSION

### 3.1 Characterization of the as-prepared PANI-doped $Li_3V_2(PO_4)_3$

Fig. 1 shows the XRD patterns of the prepared samples. The XRD patterns for the PANI-doped $Li_3V_2(PO_4)_3$, as shown by pattern **b, c** and **d**, are very consistent with the XRD pattern for the carbon-coated $Li_3V_2(PO_4)_3$ [13], indicating that PANI-doped $Li_3V_2(PO_4)_3$ with a monoclinic structure was produced. But no carbon-related diffraction peak is detected, indicating that the residual carbon is amorphous. Interestingly, one can see that after being doped by PANI the XRD patterns altered correspondingly, strongly demonstrating that the doped PANI has an evident influence on the crystal

structure of the obtained samples. We do admit that the XRD pattern for the PANI-free $Li_3V_2(PO_4)_3$ is not similar to the reported one of $Li_3V_2(PO_4)_3$ [7], probably due to difference of preparing method. Also, it can be seen that the intensity of XRD pattern of pattern **c** is the largest one among these four XRD patterns, suggesting that the sample with 7wt % PANI has the highest crystallinity.
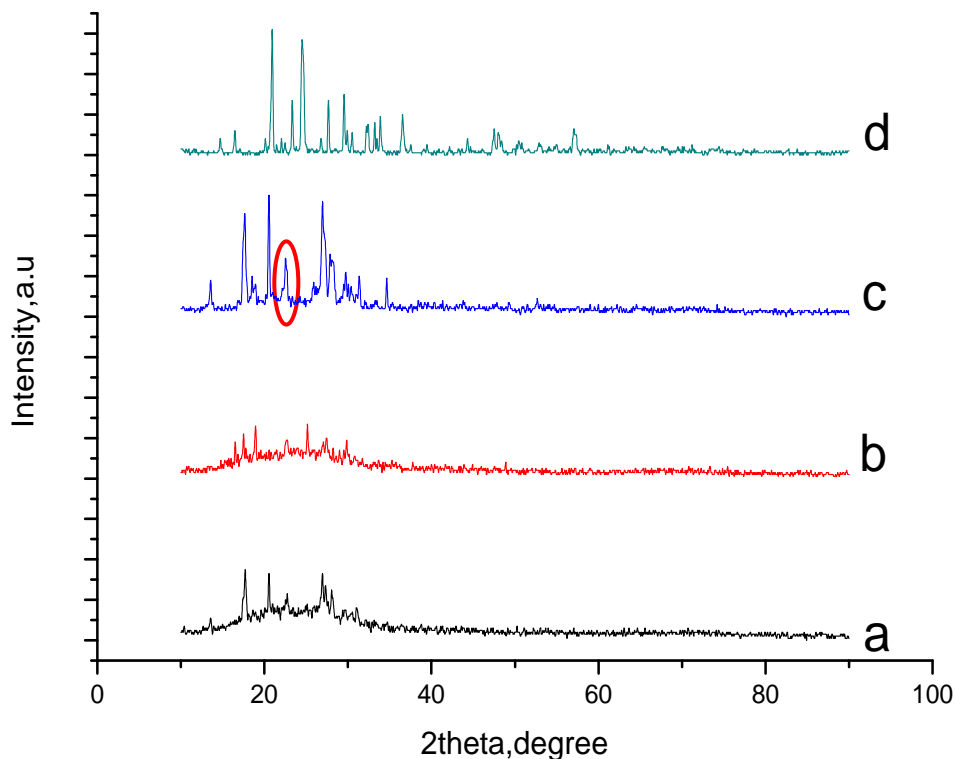
Figure 1. XRD patterns for the PANI-doped $Li_3V_2(PO_4)_3$, Pattern **a**, **b**,**c** and **d** correspond to pure $Li_3V_2(PO_4)_3$, 5wt%, 7wt% and 10 wt%-doped $Li_3V_2(PO_4)_3$, respectively.

Fig. 2 shows the SEM microstructures of the as-prepared samples. As shown by image **a**, pure $Li_3V_2(PO_4)_3$ is observed to be irregular and layered particles, while for PANI-doped $Li_3V_2(PO_4)_3$, more regular and ball-shaped particles are observed. For instance, when the weight content of PANI is about 7%, as shown by image **c**, more regular and smaller particles are displayed. Interestingly, for the 10wt% PANI-doped $Li_3V_2(PO_4)_3$, as shown by image **d**, larger particles are clearly observed. The morphology of 7wt% PANI-doped $Li_3V_2(PO_4)_3$ is almost identical to that of the reported $Li_3V_2(PO_4)_3$ [14], in which $Li_3V_2(PO_4)_3$ was prepared by a sol–gel method under Ar/H_2 (8% H_2) atmosphere using $LiOH \cdot H_2O$, NH_4VO_3, H_3PO_4 and citric acid as the raw materials. Obviously, the particle size of 7wt% PANI-doepd $Li_3V_2(PO_4)_3$ is the smallest one among the obtained samples. As reported by Gaberscek et al [15], the smaller size favors the intercalation/de-intercalation process of the Li ions and the discharge capacity drops more or less linearly with increasing the particle size. Thus, SEM image of 7wt% PANI-doepd $Li_3V_2(PO_4)_3$ may imply its promising electrochemical performance.
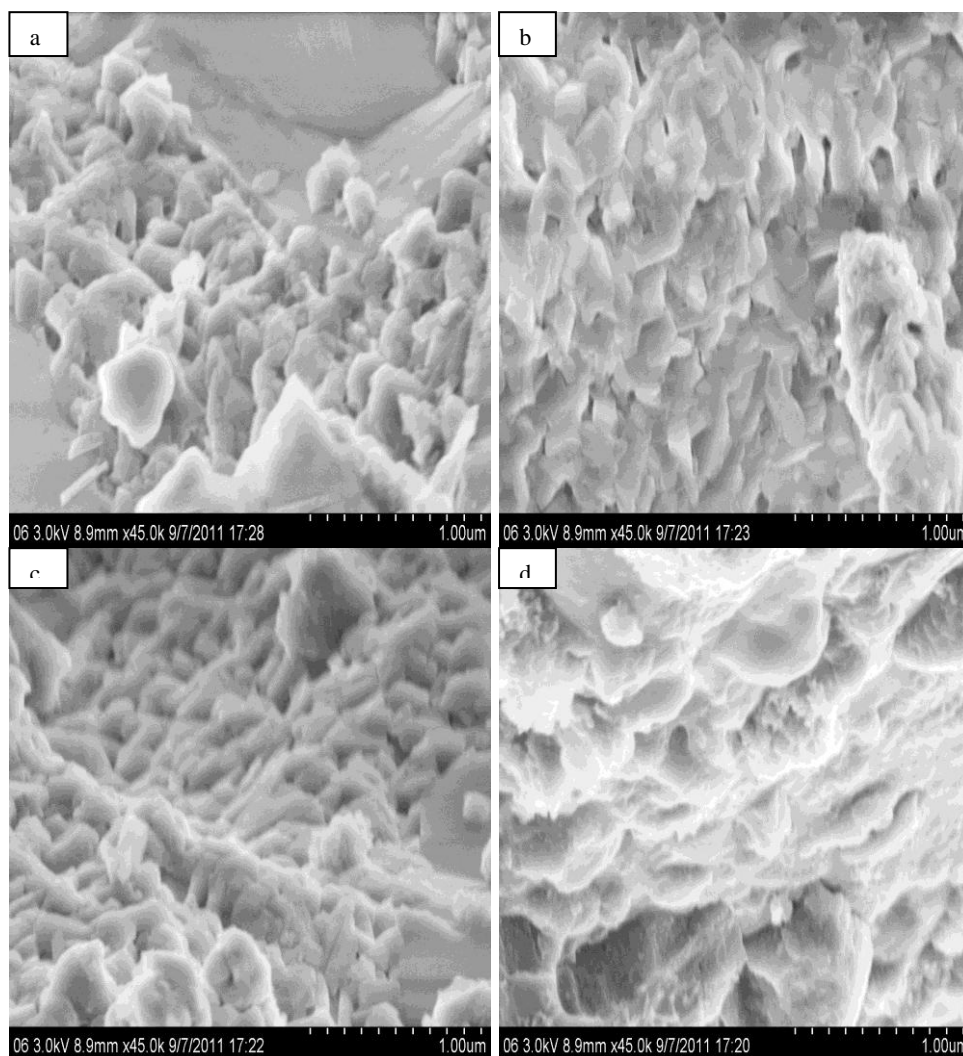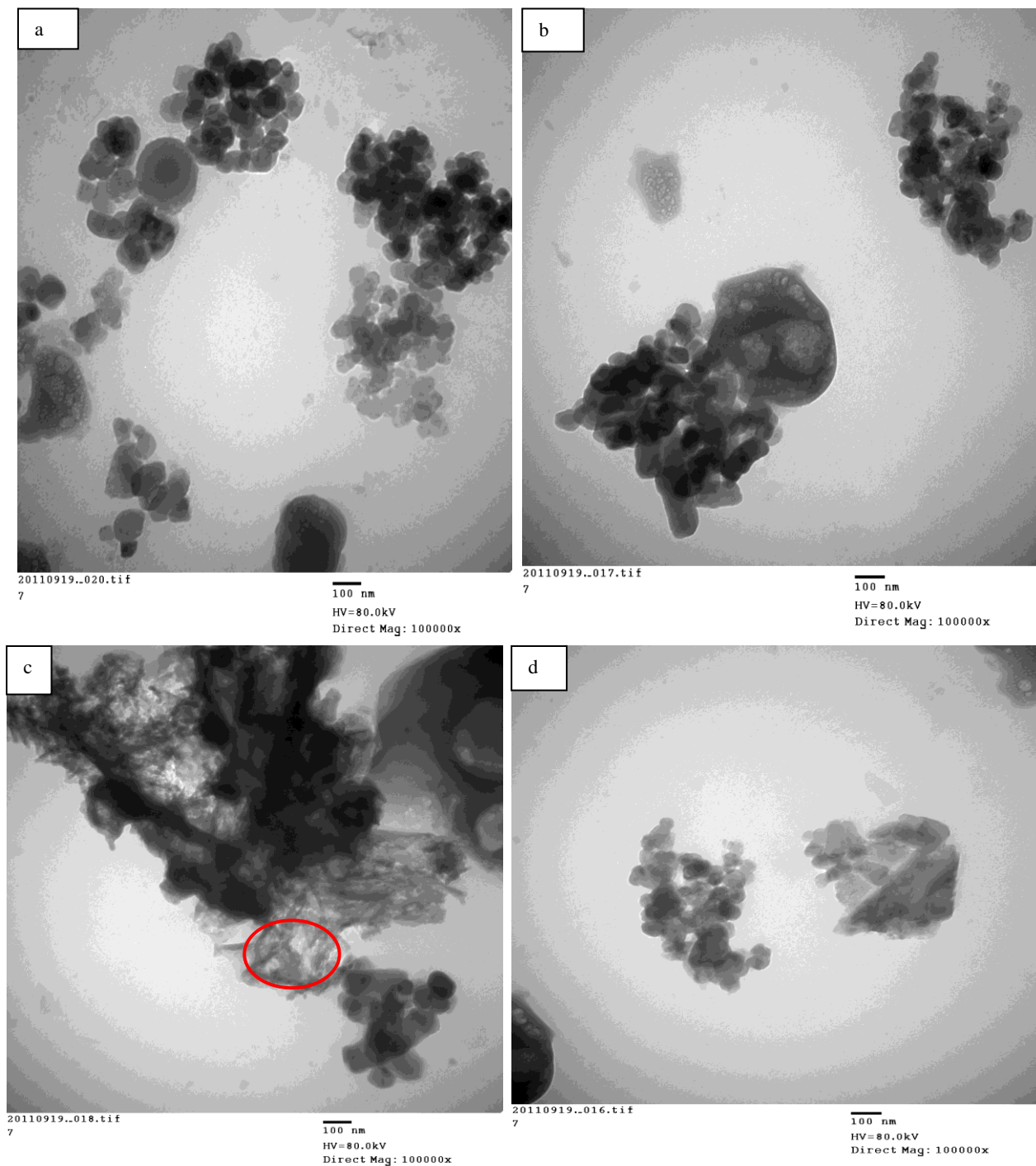
Figure 2. SEM images for the obtained samples. Image **a**: pure $Li_3V_2(PO_4)_3$. **b**, **c**, and **d** are for 5, 7 and 10 wt%-doped $Li_3V_2(PO_4)_3$, respectively.

Fig. 3 shows the TEM microstructures of the obtained samples. For the pure $Li_3V_2(PO_4)_3$, irregular particles with a particle size ranging from 80 to 180 nm are observed. While for the 5wt% PANI-doped $Li_3V_2(PO_4)_3$, more larger particles are displayed, but it seemed that aggregation between particles occurred. Interestingly, for the 7wt% PANI-doped $Li_3V_2(PO_4)_3$, needle-shaped or nano-web structure are seen as shown by the red-circled part in image **c**, probably corresponding to the carbon prepared in the preparing process. It is reported that the organic precursor of oxalic acid can be converted into electronically conductive carbon through pyrolysis processes at high temperatures under inert atmospheres [7]. Thus, in this case, probably the formed carbon are produced from the co-pyrolysis process of oxalic acid and aniline, which may increase the conductivity of $Li_3V_2(PO_4)_3$, showing an improved electrochemical performance when compared to other three samples.

Fig. 4. is the EDS spectroscopy for the pure and 7wt% PANI-doped $Li_3V_2(PO_4)_3$. It can be seen from line **a** that for the pure sample, only peaks corresponding to P, V and O elements are displayed. While for the PANI-doped $Li_3V_2(PO_4)_3$, besides above peaks, peaks corresponding to C and N were also clearly observed, suggesting that N element originated from aniline was doped into the sample.

Unfortunately, according to the weight percent presented by line **b**, the molar ratio of V:P:O is 1:9:36, rather different from the theoretical value. It indicated a poor electrochemical performance of the obtained sample when compared to the reported $Li_3V_2(PO_4)_3$[14]. More problems, such as, how does the doped N element exist in the sample? And so on, will be answered in the further investigation on the PANI-doped $Li_3V_2(PO_4)_3$.
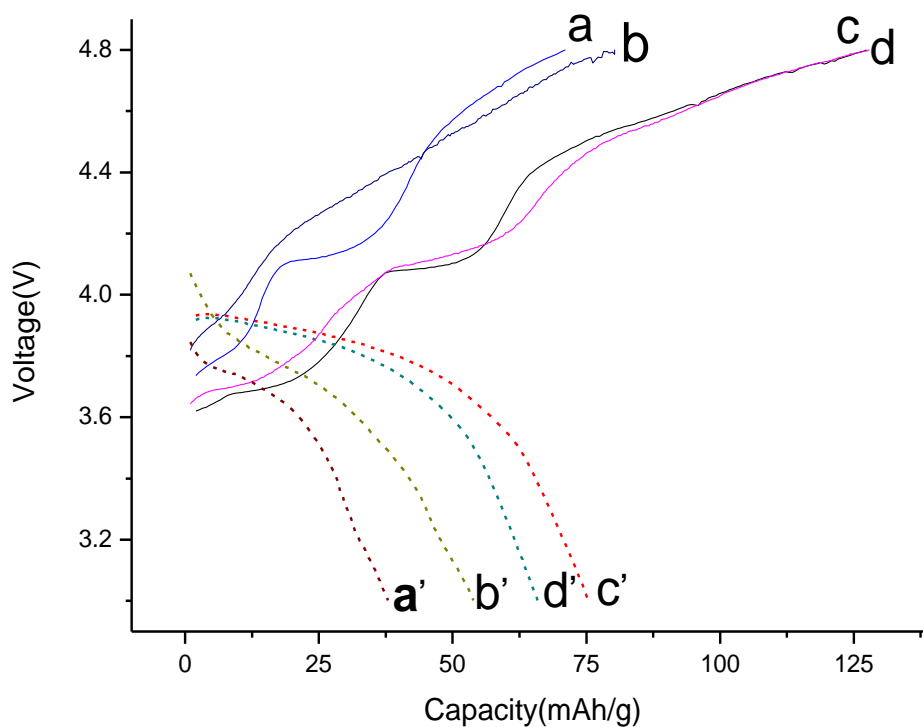

Figure 3. TEM images for the obtained samples. Image **a**: pure $Li_3V_2(PO_4)_3$. **b,c,**and **d** are for 5, 7 and 10 wt%-doped $Li_3V_2(PO_4)_3$, respectively.
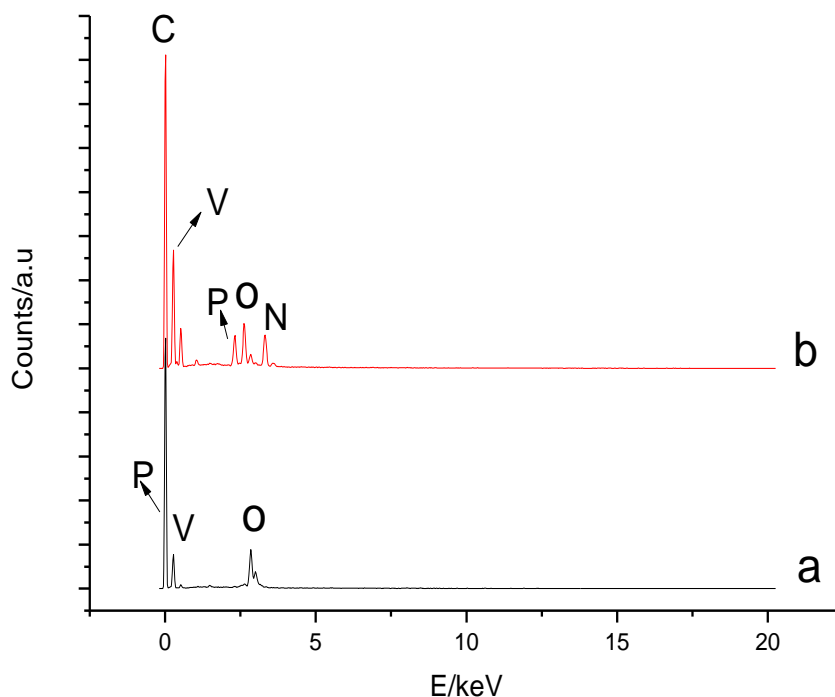
Figure 4. EDS Patterns of $Li_3V_2(PO_4)_3$(**a**) and PANI-doped $Li_3V_2(PO_4)_3$(**b**).

3.2 Electrochemical performance of the as-prepared samples

Figure 5. The first charge-discharge curves for the cells assembled by the obtained samples at 0.1C. Line **a** and **a'**, **b** and **b'**, **c** and **c'**; **d** and **d'**correspond to the pure $Li_3V_2(PO_4)_3$, 5wt%, 7 wt%, 10wt% PANI-doped $Li_3V_2(PO_4)_3$, respectively.

Fig. 5 shows the initial charge-discharge curves of the cells at 0.1 C rate using the as-prepared samples as cathodes. The cells were cycled at 0.1 C rate between 3.0 and 4.8 V vs. Li/Li$^+$. For curve **a**, there is only one plateau appearing at around 4.1V, which corresponds to the charging process of Li$_3$V$_2$(PO$_4$)$_3$. While for curve **c**, corresponding to the sample of 7wt% PANI-doped Li$_3$V$_2$(PO$_4$)$_3$, there are two plateaus appearing in the charging process, which may correspond to a two-step crystal phase transition. This preliminary work at least has demonstrated that the doping of PANI can greatly affect the charging-discharging process of the obtained Li$_3$V$_2$(PO$_4$)$_3$, though this charging behavior is poor when compared to the reported charging curve by Chen [7]. Chen reported the initial charge–discharge curves and cycling performance of LVP (Li$_3$V$_2$(PO$_4$)$_3$) /C samples with different carbon contents at the 0.5C rate in the voltage range of 3.0–4.3V, and found that there are three charge flat plateaus at around 3.65, 3.70, 4.15V and three discharge flat plateaus at around 3.5, 3.6 and 4.0V. He thought that these three pairs of plateaus correspond to two complicated phase transition processes between the single phase of Li$_x$V$_2$(PO$_4$)$_3$ (x=3.0, 2.5, 2.0 and 1.0). In this work, the initial charge capacity for Li$_3$V$_2$(PO$_4$)$_3$, 5 wt%, 7 wt%, and 10 wt% PANI-doped Li$_3$V$_2$(PO$_4$)$_3$ at 0.1 C are 71.1, 80.3, 127.9 and 126.5 mAh/g, respectively. Thus, the sample having 7wt%PANI showed the largest charge capacity among these samples. Unfortunately, different from the reported data [7], for the discharing curves, only a sloping voltage plateau was displayed in the potential range from 3.5 to 4.0V. And the initial discharge capacity for Li$_3$V$_2$(PO$_4$)$_3$, 5 wt%, 7 wt%, and 10 wt% PANI-doped Li$_3$V$_2$(PO$_4$)$_3$ at 0.1 C are only 37.9, 65.9, 75.4 and 53.9 mAh/g, respectively. Generally, the relatively large polarization and sluggish kinetics, which were resulted from the poor electronic conductivity of the cathode material, may account for the sloping voltage plateaus and the large voltage difference between the associated charge and discharge. Probably, the poor discharging hebavior displayed here are related to the lower electronic conductivity and the unsatisfactory crystal structure (as shown by XRD pattern **a** in Figure 1) of the obtained samples.
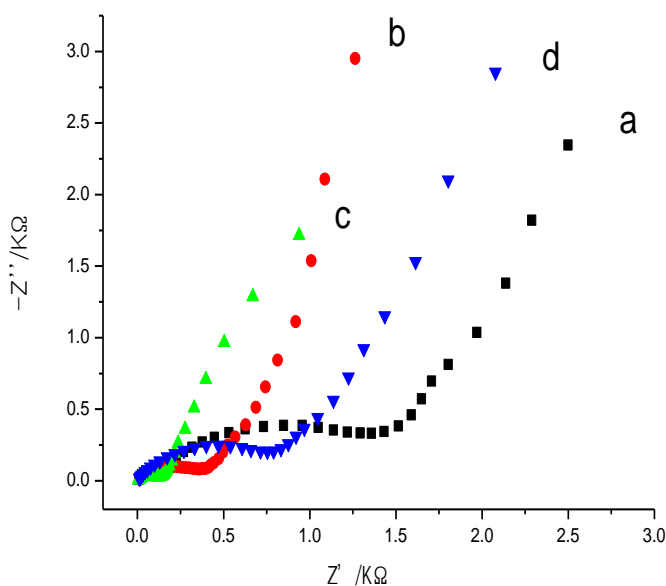
Figure 6. Nyquist plots for the cells assembled by the obtained samples at open circuit potential. Pattern a: Li$_3$V$_2$(PO$_4$)$_3$; pattern **b**: 5wt% ; pattern **c**: 7wt%; pattern **d**: 10wt%。

Electrochemical impedance spectroscopy (EIS) is one of the most powerful tools to analyze the electrochemical reactions, such as those processes occurring at the electrode/electrolyte interfaces and the lithium ion intercalation/deintercalation occurring in anode/cathode[15,16]. To discuss the role of doping PANI in $Li_3V_2(PO_4)_3$, Nyquist plots of the cells assembled by the obtained samples are shown in Figure 6. Generally, a semicircle in the medium frequency region is related to the charge transfer process and an inclined line in the low frequency region represents the Warburg impedance, which is associated with the lithium-ion diffusion in cathode materials [16]. The charge transfer resistances (R_{ct}) for $Li_3V_2(PO_4)_3$, 5 wt%, 7 wt%, and 10 wt% PANI-doped $Li_3V_2(PO_4)_3$ are estimated to be around 1600, 500, 180 and 900 Ω, respectively. This indicates that the intercalation/deintercalation process of the lithium ions in 7wt% PANI-doped $Li_3V_2(PO_4)_3$ is easier than that occurring in other samples, which is consistent with the results obtained from charge-discharge curves shown in Figure 5. Chen [7] also reported the Nyquist plots of cell assembled by the $Li_3V_2(PO_4)_3$/C samples, in which three regions, i.e., two semicircles and an inclined line, are clearly observed. He thought that the high-frequency semicircle is attributed to the migration of Li+ ions through the SEI film, whereas, the high-middle frequency semicircle represents the charge–transfer process, and the low frequency region of the inclined line corresponds to the diffusion of Li^+ ions in the bulk of the electrode material. In his work, the charge–transfer impedance for the sample $Li_3V_2(PO_4)_3$) prepared from poly(vinylidene difluoride) (noted as PVDF-sample) is about 200Ω, much lower than the value we reported here. He thought the good rate performance of PVDF-sample is attributed to a uniform carbon network with $Li_3V_2(PO_4)_3$ particles imbedded. Similarly, here, it can be seen from TEM images in Fig.3 that when the weight content of PANI is 7wt%, as shown by the red circled part, some web-shaped carbons are observed, which may greatly improve the electronic conductivity of the sample.

The lithium-ion diffusion coefficient (D) can be calculated from Equation (1) [17]

$$D = R^2T^2 / 2A^2n^4F^4c^2\sigma^2 \qquad (1)$$

where R is the gas constant, T is the absolute temperature, A is the surface area of the cathode, n is the number of electrons per molecule during oxidization, F is the Faraday constant, C is the concentration of the lithium ions (7.69×10^{-3} mol/cm^3)[18], and σ is the Warburg factor which is associated with $Z^{'}$. The lithium-ion diffusion coefficients for 5, 7, and 10wt% PANI-doped $Li_3V_2(PO_4)_3$ are calculated to be 8.5×10^{-11} , 9.6×10^{-9} , 1.1×10^{-11} cm^2/s, respectively. The D value of 7wt% PANI-doped $Li_3V_2(PO_4)_3$ is the largest one among the three samples, which may promise a higher discharge capacity value. This result can be attributed to the smaller particle size of 7wt% PANI-doped $Li_3V_2(PO_4)_3$ relative to other samples as evidenced by SEM observation, Figure 2, favoring the intercalation/de-intercalation process of the Li ions in the cathode materials. Wang's group[19] synthesized $Li_3V_2(PO_4)_3$/C cathode materials by a simple solid-state reaction process using stearic acid as both reduction agent and carbon source, in which the apparent diffusion coefficients of Li ions in the composites are in the region of 1.09×10^{-9} cm^2 s^{-1} and 4.95×10^{-8} cm^2 s^{-1}. Thus, the smaller value of D we obtained may be responsible for the poor electrochemical performance of the as-prepared samples here.

The charge-discharge curves of the cell assembled by the 7 wt% PANI-doped $Li_3V_2(PO_4)_3$ at various rates are shown in Fig. 7. The initial discharge capacities for the cell at 0.1, 0.2 and 0.5C are 75.4, 64.2, 59.3 mAh/g, respectively. It indicated that the polarization of the cell was greatly enlarged by the increased current density, leading to a lower discharge capacity value. Although the discharge capacity here is much smaller than the published data [19], it is the first time to report the preparation and electrochemical performance of PANI-doped $Li_3V_2(PO_4)_3$.
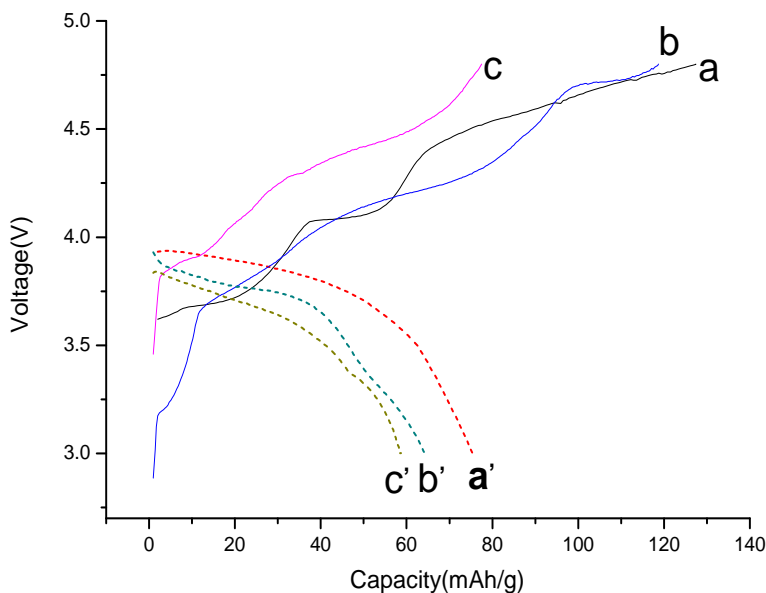

Figure 7. The first charge / discharge curves for the cells assembled by the obtained 7wt% PANI-doped $Li_3V_2(PO_4)_3$ at various rates. Line **a** and **a'**, **b** and **b'**, **c** and **c'** correspond to the rates 0.1, 0.2 and 0.5C, respectively.
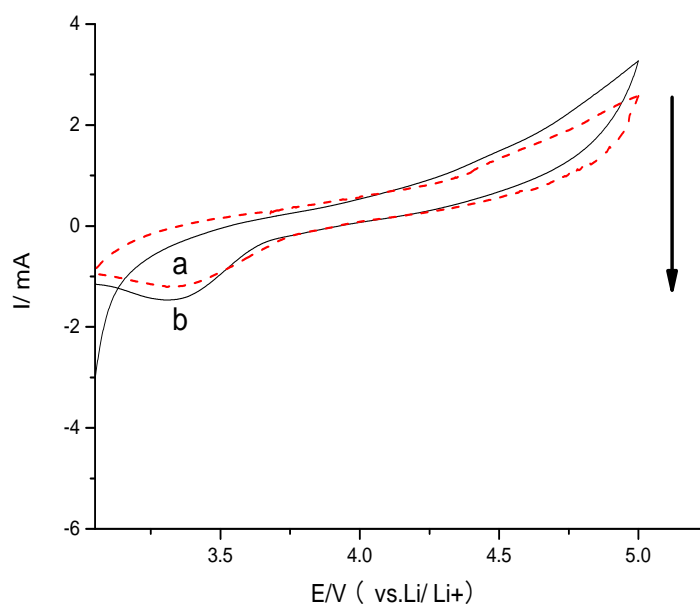
Figure 8. CVs for the cell assembled by the 7 wt% PANI-doped $Li_3V_2(PO_4)_3$ at various scan rates. Line **a**: 1.0mV/s ; line **b**:2.0 mV/s.

To analyze the reasons for the poor electrochemical perofrmance, cyclic voltammograms (CVs) of the cells assembled by the 7 wt% PANI-doped are shown by Fig. 8. One can see that only a reduction peak was displayed in the potential rang from 3.0 to 4.8V, and the well-defined redox peaks corresponding to the intercalation/de-intercalation of the lithium ions were not observed. It indicates that Li ions can not intercalate/deintercate in/from the as-prepared PANI-doped $Li_3V_2(PO_4)_3$ freely. In the positive direction potential scanning, no oxidation peaks were found, suggesting that Li+ can not easily extract from the cathode materials, probably the lone electron pair in the element of N inhibited the releasing process of Li+ from the cathode materials. While, in the negative direction potential scanning, the reduction peak was well displayed, indicating that Li+ can intercalate into the cathode materials easily. Therefore, there is a sloping voltage plateau in the discharging process. Also, one can see that the reduction peak current enhanced greatly with the scanning rate, indicating that the diffusion process exist in the charge-discharge process, though unsatisfactory electrochemical performance was displayed. How do we understand this phenomenon? More works should be done to reveal the exact interaction between the Li+ and the cathode materials.
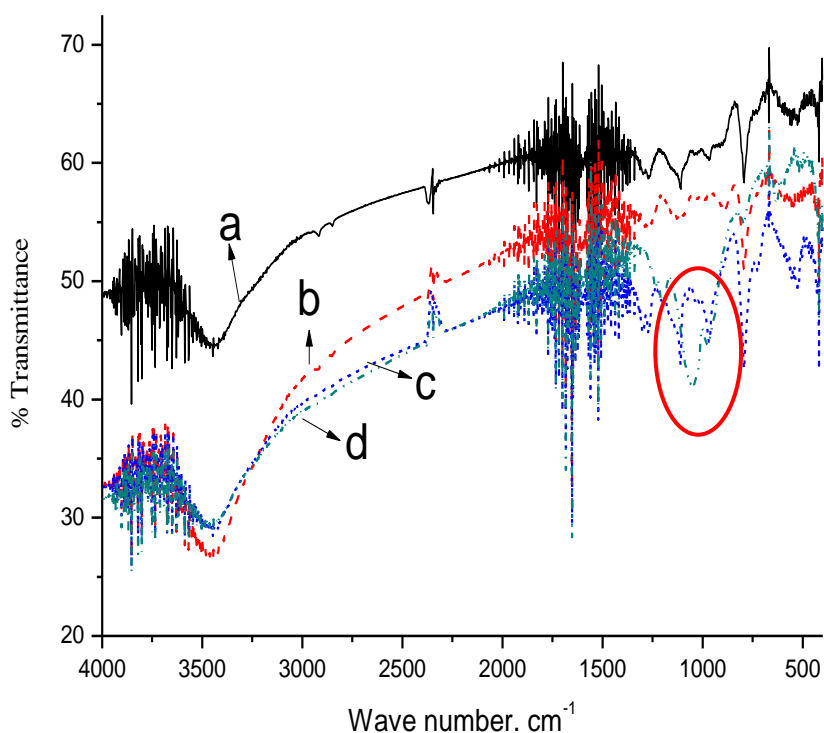
Figure 9. FTIR spectra for the PANI-doped $Li_3V_2(PO_4)_3$. Curve **a**: $Li_3V_2(PO_4)_3$; The content of PANI of curve **b**, **c** and **d** are 5wt% , 7wt% and 10wt%, respectively.

To discuss the influence of PANI doping on the obtained samples, FT-IR spectra for all the samples were recorded, Figure 9. Generally, the peak at 3410cm^{-1} can be ascribed to –OH group of adsorbed water molecules. The characteristic peaks at 1580cm^{-1} and 1500cm^{-1} correspond to the quinoid ring (Q) and the benzene ring, respectively. The bands in the range 1200–1400cm are the C–N

stretching band of an aromatic amine. The characteristic band of polyaniline base is the N=Q=N stretching band at 1130cm^{-1}[20]. One can see that with the increase of PANI content, as shown by the red circles part, the band at 1130 cm^{-1} became distinct, suggesting more N were doped into $Li_3V_2(PO_4)_3$. That is to say, PANI played an important role on the electrochemical performance of our prepared samples.

4. CONCLUSION

For the first time, the PANI-doped $Li_3V_2(PO_4)_3$ was prepared by an improved solid state reaction. And the obtained samples were thoroughly characterized by XRD, SEM and TEM. It was revealed that the doping of PANI can affect the crystallinity of the as-prepared samples, and the particle size as well. Charge-discharge curves indicated that the 7wt% PANI-doped $Li_3V_2(PO_4)_3$ showed the largest discharge capacity among the prepared samples, though the discharge capacity is much lower than the theoretical discharge capacity value. CVs of the cell also demonstrated that no evident redox peaks were observed, which can largely account for the poor electrochemical performance of the PANI-doped $Li_3V_2(PO_4)_3$. Presenting the preparation of PANI-doped $Li_3V_2(PO_4)_3$ by a carbon-coated crucible is the main contribution of this preliminary work.

References

1. S.-B. Yi , H.-T. Chung , H.-G. Kim, *Electrochem. Commun.,* 9 (2007) 591
2. B. Kang, G. Ceder, *Nature* 458 (2009) 190
1. 3.Q.Q.Chen,J.M.Wang,Z.Tang,W.C.He,H.B.Shao,J.Q.Zhang, *Electrochim.Acta* 52 (2007) 5251.
3. H. Huang, T. Faulkner, J. Barker, M.Y. Saidi, *J. Power Sources* 189 (2009)748.
4. L. Zhang, X.L. Wang, J.Y. Xiang, Y. Zhou, S.J. Shi, J.P. Tu, *J. Power Sources* 195 (2010) 5057.
5. Q. Kuang, Y. Zhao, X. An, J. Liu, Y. Dong, L. Chen, *Electrochim.Acta* 55 (2010) 1575.
6. X.H. Rui, C. Li, C.H. Chen, *Electrochim. Acta* 54 (2009) 3374.
7. J.X. Huang, S. Virji, B.H. Weiller, R.B. Kaner, *J. Am. Chem. Soc.*, 125 (2003) 314.
8. S. Neves , C. Polo Fonseca, *J.Power Sources* 107 (2002) 13.
9. K. Ghanbari, M. F. Mousavi , M. Shamsipur, H. Karami, *J. Power Sources* 170(2007)513.
10. W.-M. Chen, L. Qie, L.-X. Yuan, S.-A. Xia, X.-L. Hu, W.-X. Zhang, Y.-H. Huang, *Electrochim. Acta* 56 (2011) 2689.
11. K.-Q. Ding, *J. Chin. Chem. Soc.,* 56(2009) 891.
12. C. Chang, J. Xiang, X. Shi, X. Han, L. Yuan, J. Sun, *Electrochim. Acta* 54 (2008) 623.
13. X.J. Zhu, Y.X. Liu, L.M. Geng, L.B. Chen, *J. Power Sources* 184(2008)578.
14. K. Ding, Z.Jia, Q.Wang, X.He, N.Tian, R.Tong, X. Wang, *J. Electroanal. Chem.*, 67(2001) 513.
15. Y.Q. Qiao, J.P. Tu, X.L. Wang, D. Zhang, J.Y. Xiang, Y.J. Mai, C.D. Gu, J. Power Sources 196

(2011) 7715.
16. A.J. Bard, L.R. Faulkner, *Electrochemical Methods*, second ed., Wiley, 2001, p. 231.
17. B. Jin , E. M. Jin , K.-H. Park , H.-B. Gu, *Electrochem. Commun.* 10 (2008) 1537
18. Y.Q. Qiao, X.L. Wang, J.Y. Xiang, D. Zhang, W.L. Liu, J.P. Tu, *Electrochim. Acta* (2010), doi:10.1016/j.electacta.2010.11.073
19. Y.-G. Wang, W. Wu, L. Cheng, P. He, C.-X. Wang, Y.-Y. Xia, *Adv. Mater.,* 20 (2008) 2166
20. Y.-G. Wang, H.-Q. Li, Y.-Y. Xia, *Adv. Mater.,* 18 (2006) 2619